

The zero-temperature phase diagram of soft-repulsive particle fluids

Santi Prestipino¹ [*], Franz Saija² [†], and Gianpietro Malescio¹ [‡]

¹ *Università degli Studi di Messina, Dipartimento di Fisica,
Contrada Papardo, 98166 Messina, Italy*

² *CNR-Istituto per i Processi Chimico-Fisici,
Contrada Papardo, 98158 Messina, Italy*

(Dated: November 1, 2018)

Abstract

Effective pair interactions with a soft-repulsive component are a well-known feature of polymer solutions and colloidal suspensions, but they also provide a key to interpret the high-pressure behaviour of simple elements. We have computed the zero-temperature phase diagram of four different model potentials with various degrees of core softness. Among the reviewed crystal structures, there are also a number of non-Bravais lattices, chosen among those observed in real systems. Some of these crystals are indeed found to be stable for the selected potentials. We recognize an apparently universal trend for unbounded potentials, going from high- to low-coordinated crystal phases and back upon increasing the pressure. Conversely, a bounded repulsion may lead to intermittent appearance of compact structures with compression and no eventual settling down in a specific phase. In both cases, the fluid phase repeatedly reenters at intermediate pressures, as suggested by a cell-theory treatment of the solids. These findings are of relevance for soft matter in general, but they also offer fresh insight into the mechanisms subtended to solid polymorphism in elemental substances.

PACS numbers: 61.50.Ks, 61.66.Bi, 62.50.-p, 64.70.K-

Keywords: High-pressure effects in solids, Reentrant melting, Phase diagram of the elements

I. INTRODUCTION

Soft-matter systems, like solutions of polymer chains or dispersions of colloidal particles, have been the subject of increasing interest in the last few decades owing to the possibility they offer of exploring new kinds of equilibrium phase behaviour which radically depart from the simple-fluid paradigm as exemplified by rare gases [1, 2]. In the reduced-Hamiltonian approach, all of the colloid degrees of freedom are integrated out, except for the centre-of-mass coordinates which are taken to interact via an effective potential energy U . A further simplification occurs upon restricting the form of U to a sum of two-body spherically-symmetric contributions, $U = \sum_{i < j} u(r_{ij})$, r_{ij} being the distance between particles i and j . It turns out that the $u(r)$ potential is typically softer (i.e., characterized by a less steep short-range repulsion) than, say, the Lennard-Jones potential, if not even being finite for vanishing interparticle distance as a result of full interpenetrability of the mesoscopic particles.

A well-studied case is that of star polymers, i.e., colloidal particles with a more or less hard inner core surrounded by a soft penetrable corona made of grafted polymer chains. For those distances where coronas overlap, the effective repulsion between two stars grows only logarithmically with reducing distance, leading to stabilization of low-coordinated crystals in a range of densities [3, 4]. Another much-studied system is self-avoiding polymers, which are instead fully penetrable and roughly described by a simple Gaussian repulsion [5]. At low temperature, the Gaussian-core model (GCM) can exist in two distinct crystal phases of the face-centred cubic (fcc) and body-centred cubic (bcc) type [6, 7, 8]. Moreover, the fluid phase regains stability on increasing pressure at constant temperature (reentrant melting) due to an overwhelmingly larger number, at same energy, of spatially disordered configurations over crystalline ones.

Simple elements under extreme thermodynamic conditions provide another instance of a soft short-range repulsion between the system constituents [9]. In this case, the softness of the effective repulsion is ultimately a reflection, on a coarse-grained level, of a pressure-dependent atomic radius, as determined in turn by pressure-induced charge transfer between atomic orbitals. These effects are well understood in the case of alkali metals, whose electronic structure at high pressures departs radically from nearly free-electron behaviour and their common low-pressure symmetric structure (bcc) becomes unstable to pairing of the ions. While it could generally be argued that the use of a classical interatomic potential is

not permitted for most elemental liquids and solids, owing to the fact that electronic effects are important and are even strongly enhanced by the pressure, a classical framework for the study of the phase behaviour of simple substances is still possible, in the same spirit of the Born-Oppenheimer separation between nuclear and electronic degrees of freedom in molecules. Non-adiabatic effects are truly negligible for insulators and semiconductors but seemingly not so for metals where the absence of a gap between occupied and unoccupied states would make the adiabatic approximation not particularly well justified. However, the fraction of electrons that can be scattered by phonons is rather small even at room temperature since electrons that lie sufficiently far from the Fermi surface remain frozen in their states by Pauli's principle. Hence, the notion of an adiabatic potential as well as the very same concept of a crystal remain meaningful also for normal metals. This conclusion can be made rigorous by a theorem due to Migdal [10].

In a recent publication [9], we have sketched the overall phase diagram of a system of point particles interacting through the exp-6 (Buckingham [11]) potential, which is being used since long time as an effective description of rare gases and metals under extreme conditions [12, 13, 14]. In spite of such popularity, important features of the exp-6 phase behaviour had previously passed unnoticed. In particular, the reentrant-melting behaviour, similar to the GCM model, and the rich solid polymorphism, both a generic trait of elemental substances at high pressures [15]. In the exp-6 system, reentrant melting and solid polymorphism are both manifestations of the statistical competition, as a function of pressure, between two distinct scales of nearest-neighbour distance [9]. These two length scales arise as a result of the radial dependence of the exp-6 repulsion, which shows a range of distances where the force strength *diminishes* with decreasing interparticle separation (indeed, a rather strong form of core softness). Whence two preferred values of the mean neighbour distance and the ensuing frustration of crystalline packing of the standard (fcc or bcc) type in a certain pressure range.

In this paper, we shall be concerned with the relation between softness of the interparticle repulsion and polymorphism of the solid phase, with an emphasis on the occurrence of thermodynamically stable non-Bravais crystals. We consider four distinct model potentials that have already appeared in the literature, so as to cover a wide range of possibilities. Aside from the degree of softness, the chosen potentials differ as for having or not a hard core as well as for diverging or not at zero separation. In all cases, we provide an accurate

analysis of the zero-temperature ($T = 0$) phase diagram by examining a large number of potentially relevant structures, much larger than ever considered before (at least for these potentials). In particular, we provide an update of the $T = 0$ behaviour of the exp-6 potential as being reported in Ref.[9]. We know of only a few studies of a similar kind where the search for stable structures was carried out more systematically (by e.g. a genetic algorithm) [16, 17, 18, 19, 20], but neither regarded the potentials hereby analysed.

The rest of the paper is organized as follows: In Section 2, we introduce the potentials for which the $T = 0$ phases are computed. Then, in Section 3, we give a brief description of the crystal structures being analysed and briefly outline the numerical technique that we use to optimize a specific structure for a given pressure. Results for the different potentials are presented in Section 4, with an attempt to find a common thread among them. Some further remarks and conclusions are given in Section 5.

II. SOFT-CORE POTENTIALS

Model potentials that describe the effective pair interaction between particles of simple atomic fluids have a short-range repulsive component whose steepness (i.e., absolute slope) diverges at zero separation as an effect of the increasing hindrance, implied by the exclusion principle, to making particles more and more close to each other. In Lennard-Jones and inverse-power fluids, the repulsive force ($\equiv -u'(r)$) steadily increases, with an ever increasing rate, as particles get closer. By contrast, in soft-core potentials the repulsive force, or at least the rate with which the force increases, is not a monotonous function of r .

The first soft-core potential we want to consider is the exp-6 potential

$$u_E(r) = \begin{cases} +\infty & , \quad r < \sigma_M \\ \frac{\epsilon}{\alpha-6} \left\{ 6 \exp \left[\alpha \left(1 - \frac{r}{\sigma} \right) \right] - \alpha \left(\frac{\sigma}{r} \right)^6 \right\} & , \quad r \geq \sigma_M \end{cases} \quad (2.1)$$

where ϵ is the depth of the attractive well, σ is the position of the well minimum, $\alpha > 7$ is a parameter governing the steepness of the short-range repulsion, and σ_M is the point where the function in Eq. (2.1) attains its maximum. This interaction was already studied in some detail for the case $\alpha = 11$ in [9], where we also provided a sketch of the phase diagram at $T = 0$. However, in that paper only a relatively small number of crystal structures were scrutinized. We here extend that study and find other crystals with a smaller chemical potential in a certain pressure range.

The exp-6 potential as well as the Gaussian repulsion are instances of strongly-soft repulsions in that the force slope is *positive* in a range of distances. However, we can also devise soft-core potentials whose force always increases upon reducing the interparticle distance while the force steepness does not monotonously increase as well. This is e.g. the case of the potential

$$u_{YK}(r) = \epsilon \exp \left\{ a \left(1 - \frac{r}{\sigma} \right) - 6 \left(1 - \frac{r}{\sigma} \right)^2 \ln \left(\frac{r}{\sigma} \right) \right\}, \quad (2.2)$$

where $a = 2.1$. This potential was first introduced in Refs. [21, 22], and will thus be referred to as the Yoshida-Kamakura potential. A limited study of the $T = 0$ phase diagram of this model was already presented in Ref. [23]. The force $-u'_{YK}(r)$ always increases with reducing r but it does so at a somewhat smaller rate in a range of distances around σ where $u''_{YK}(r)$ develops a local minimum (see Fig. 1).

We consider two other model potentials that have recently been studied in the literature. These are the smoothed hard-core plus repulsive-step (Fomin) potential [24],

$$u_F(r) = \left(\frac{\sigma}{r} \right)^{14} + \frac{\epsilon}{2} \left[1 - \tanh \left(10 \frac{r - r_0}{\sigma} \right) \right], \quad (2.3)$$

with $r_0 = 1.35 \sigma$, and the interaction potential of compressed elastic (Hertzian) spheres [25],

$$u_H(r) = \begin{cases} \epsilon \left(1 - \frac{r}{\sigma} \right)^{5/2}, & r \leq \sigma \\ 0 & , \quad r > \sigma \end{cases} \quad (2.4)$$

The main reason for considering these potentials is that an accurate analysis of the phase diagram was performed for both. Reentrant melting and solid polymorphism are observed in both cases but, as we shall see, not all stable low-temperature phases were actually identified. Moreover, while $u_F(r)$ is a strongly-soft potential that, at variance with the exp-6 potential, lacks a strictly hard core, $u_H(r)$ is a bounded potential that, unlike the Gaussian repulsion, does not fit our definition of soft-core potential. This may appear strange since, for bounded repulsions, two particles can sit on top of each other – a fact which by itself is indication of the intrinsic “softness” of the interaction.

To highlight the soft nature of the Hertz potential, we look at the r -dependence of what we call the effective inverse-power exponent (EIPE) of a potential. The EIPE of $u(r)$ is defined as the value of n in $u_{IP}(r) = A/r^n$ which provides the best local matching between $u_{IP}(r)$ and $u(r)$ [26]. By imposing the equality of the functions and their derivatives at a fixed r , we find

$$n(r) = - \frac{r u'(r)}{u(r)}. \quad (2.5)$$

In Fig. 2, we report $n(r)$ for the potentials (2.1)-(2.4) (for the sake of clarity, we have made the discontinuity of $u_E(r)$ at σ_M milder by replacing the hard core with an extremely steep power-law barrier). We see indeed that, for all potentials, $n(r)$ decreases significantly for decreasing r in a range of r values, thus signalling core softening and pointing at the same time to the existence of similarities among the four models as for the low- to moderate-pressure phase behaviour.

We now prove, by adapting an argument originally due to Stillinger [6], that a system of particles interacting through either $u_{YK}(r)$ or $u_F(r)$ is found in a stable fcc crystal for sufficiently low densities and temperatures, as indeed suggested by the divergence of the EIPE at infinity. Let $u(r) \equiv \epsilon\psi(r/\sigma)$ be a purely repulsive and monotonously decreasing potential. The Boltmann's factor for a pair of particles is

$$b(r_{ij}) = \exp \left\{ -\frac{\psi(r_{ij}/\sigma)}{\psi(R/\sigma)} \right\}, \quad (2.6)$$

with $R = \sigma\psi^{-1}(k_B T/\epsilon)$, k_B being Boltzmann's constant (note that the distance R diverges as the temperature T goes to zero). We now calculate the $T = 0$ limit of $b(xR)$,

$$f(x) \equiv \lim_{T \rightarrow 0} b(xR) = \exp \left\{ -\lim_{R \rightarrow \infty} \frac{\psi(xR/\sigma)}{\psi(R/\sigma)} \right\}. \quad (2.7)$$

For

$$\psi(R/\sigma) \sim \begin{cases} \exp\{-6(R/\sigma)^2 \ln(R/\sigma)\} & \text{(Yoshida - Kamakura potential)} \\ \exp\{-\gamma R/\sigma\} & \text{(Fomin potential)}, \end{cases} \quad (2.8)$$

one invariably has

$$f(x) = \begin{cases} 0^+ & , \quad 0 < x < 1 \\ 1/e & , \quad x = 1 \\ 1^- & , \quad x > 1 \end{cases} \quad (2.9)$$

In other words, at very low temperature $u(r)$ reduces practically to the hard-sphere potential and exactly so in the limit $T \rightarrow 0$. Correspondingly, R plays the role of an effective hard-core diameter. Since the values of the hard-sphere packing fraction at freezing and melting are well known [27], the lines of fluid-fcc coexistence are implicitly given by the equations

$$\frac{\pi}{6} (\rho R(T)^3)_f = 0.492 \quad \text{and} \quad \frac{\pi}{6} (\rho R(T)^3)_m = 0.543, \quad (2.10)$$

which become rigorously valid in the limit $T \rightarrow 0$.

III. CRYSTAL LATTICES AND THEIR SCRUTINY

At $T = 0$ and fixed pressure, a (crystal) phase is thermodynamically stable if its chemical potential is smaller than that of any other phase at equal pressure. We are then faced with the problem of minimizing the enthalpy per particle as a function of pressure among *all* possible crystals. This is a formidable problem, since the possibilities are virtually infinite. Hence, we restrict our search of stable structures to a limited albeit large number of candidates including, aside from Bravais crystals, also a number of Bravais lattices with a basis (i.e., non-Bravais lattices) that have been demonstrated to be relevant for some soft material or simple substance under high pressures. We do not anyhow consider the possibility for phases made up of clusters, columns, or lamellae, which can appear if the potential exhibits two competing length scales of considerable difference (see e.g. Ref. [19]). We are fully aware of the limitations of our approach which, besides assuming a preselected set of structures, also undergoes increasing difficulties when managing lattices with many (five or more) characteristic parameters. In this respect, an approach which employs metadynamics [28, 29] or a genetic algorithm [30, 31, 32] as a tool for an automated search of optimal solutions inside the structure space would ensure a higher rate of success.

However, provided the number of crystal lattices being examined is sufficiently large, direct optimization of structures from a finite set offers the advantage of weighing up the relative stability between the optimum solution for a given pressure and the metastable crystals that crowd around it. Moreover, features like the trend of particle coordination as a function of pressure or the characteristic distances at which nearest and next-nearest particles are preferentially located around a central particle can anyway be grasped by this method.

The crystal lattices that we analyse can be divided in groups of increasing optimization difficulty, according to the number (from zero to five) of independent parameters (i.e., axial ratios, angles, and/or atomic-site parameters), besides the number density ρ , that need to be adjusted in order to minimize the enthalpy at fixed pressure. For non-Bravais lattices, these parameters are listed in Table 1, along with the number of inequivalent sites (NIS) of the lattice, defined as the maximum number of sites whose environments look different as for the population and/or radius of at least one coordination shell. For a Bravais lattice one has NIS=1, but there also exist non-Bravais lattices with this property (e.g. diamond).

The simplest close-packed structures, fcc and hexagonal close packed (hcp), are well known. In the $[111]$ direction, the stacking sequence of triangular layers is ABC for fcc and AB for hcp (the bcc lattice can also be built this way, by suitably spacing the layers one relative to the other in the same ABC sequence as for fcc). More generally, one can consider so-called Barlow packings (i.e., the stacking variants of fcc and hcp packings) where each additional layer involves a binary choice for how to place it relative to the previous layer. Among them, we consider the double hcp (dhcp) structure (stacking sequence: ABAC), which is the structure of α La, the triple hcp (thcp) structure (stacking sequence: ABCACB), and the 9R structure of δ Sm and α Li [36] (stacking sequence: ABCBCACAB). Another simple structure with no parameters is the diamond lattice (a fcc lattice with a basis of two atoms), which provides the low-pressure ground-state configuration of C, Si, Ge, and Sn. Structures with zero parameters are also the simple-cubic (sc) lattice, the one-species analog of the fluorite (CaF_2) lattice, the A15 lattice (i.e., the structure of β W, whose conventional unit cell contains eight atoms), and the bcc12 lattice (i.e., the structure of the metastable Ga-II phase).

The group of lattices with one free parameter includes, besides a few Bravais lattices (sh, st, bct, and trig – i.e., the simple rhombohedral or hR1 lattice), also the β Sn lattice (occurring also for Si, Ge, Rb, and Cs), the graphite lattice, as well as two cubic lattices obtained by suitably distorting a bcc supercell (cI16-Li [37] and BC8, both with a conventional unit cell containing eight atoms). hR1 is obtained by stretching the sc lattice along a body diagonal. The straining parameter h is usually defined [33] in such a way that $h = 0$ gives the sc lattice, $h = -1/6$ the bcc lattice, and $h = 1/3$ the fcc lattice. Both Hg and Li display a hR1 solid phase. The conventional unit cell of β Sn is tetragonal with 4 atoms inside. A cI16 phase has recently been identified also for Na [38, 39] while BC8 provides a low-pressure metastable phase for Si. The coordinates of the atoms inside the conventional unit cells of cI16-Li and BC8 are written in terms of a parameter x ranging from 0 (giving back the bcc lattice in the cI16-Li case) to $1/8$.

Aside from the Bravais lattices so, sfco, bco, and fco, crystal structures with two adjustable parameters are also the one-species analog of wurtzite (ZnS) and the so-called *Imma* phase of Si (Si-XI, stable between 13 and 16 GPa). The *Imma* phase is a distortion of β Sn. Moreover, we consider: the β Np structure, which is the one-species analog of PbO (A_d , tP4); the α As structure (A7, hR2), also relevant for Sb and Bi, which can also be viewed

as an orthorhombic lattice with $b/a = \sqrt{3}$ and a 12-atom basis; the γ Se structure (A8, hP3), also observed in Te; the β Mn structure (A13, cP20); and, finally, the C6 structure of Ti, Zr, and Hf (ω phase, hP3).

There are two further Bravais lattices with three parameters (sm, sfcu) and one with five parameters (tric). We also consider another three-parameter lattice (A20, oC4, $Cmcm$ space group), which provides the structure of α U, β Ga, and γ Ti, a four-parameter lattice (A11, oC8, $Cmca$ space group), and two more five-parameter lattices (oC16-Cs and ST12). The A11 lattice is the structure of α Ga (black P and B above 90 GPa have a similar structure). A oC8 phase was first predicted for compressed Li by Neaton and Ashcroft [40] and later confirmed by Hanfland *et al.* [37]. Theoretical calculations by Christensen and Novikov have predicted the existence of a stable oC8 phase also for Na above ≈ 250 GPa [41]. The orthorhombic oC16 lattice provides the structure of Cs-V [35] and Rb-VI but it is also observed in Si (between 38 and 45 GPa) and in Ge. Its $Cmca$ structure contains two types of atom, say A_1 and A_2 , with A_1 in planar arrangements separating A_2 double layers. Within the planes, atoms form a dense packing of dimers. The $Cmca$ structure of oC8 is similar to oC16 but the double layers of A_2 atoms are absent. Of $Cmca$ symmetry is also the structure of Ca-V [42], which has the highest superconducting transition temperature (25 K) among all the elements. Finally, ST12 denotes a simple-tetragonal metastable phase of Si with a 12-atom basis.

Let us now briefly outline the procedure we follow in order to optimize a given crystal structure for assigned potential. Loosely speaking, we make a grid of points in parameter space on which we search for the minimum enthalpy at given pressure. We consider lattices with a number of sites between 8000 and 10000, with periodic boundary conditions. Lattice sums are extended up to a cutoff distance equal to half the shortest box length for orthogonal cells (half the shortest distance of centre to boundary for non-orthogonal cells). Then, a long-range correction is added to the energy by assuming a radial distribution function (RDF) of 1 for the distant sites. We start by performing a series of harsh minimizations on rather coarse meshes but then we refine the calculation by progressively reducing the mesh size until the lattice providing the minimum chemical potential is extracted out of a number of deeper valleys in parameter space (steepest-descent methods would not necessarily be of help in this case since one could easily get stuck in local minima). We feel satisfied when we obtain the density with three exact decimal digits and the other parameters with two to

three decimals. Occasionally, we resolve near degeneracies by going to larger lattices and better parameter refining. When more than one crystal structure is found to give practically the same minimum chemical potential, we check the identity of the subtended lattices by looking at the discrete RDF of each.

IV. RESULTS AND DISCUSSION

The $T = 0$ phase diagram of model systems interacting through the soft-core potentials (2.1)-(2.4) is reported in Tables 2 to 5. Overall, we see the existence of a rich solid polymorphism, with many exotic lattices providing stable phases at moderately high pressures. Obviously, we cannot exclude that there might exist other phases which overcome in stability some of those found (to be sure, one should perform a molecular-dynamics simulation of the system at fixed pressure, starting from the high-temperature fluid and cooling it down very slowly until the solid nucleates – but the conditions for observing ideal freezing are hardly achieved in a reasonable amount of computer time). In this respect, the case of Na is particularly illuminating [39]: if the experiment does not lie, no theoretical study could ever have anticipated the bunch of crystal phases, some of which extremely complex, that Na exhibits for pressures above 110 GPa. Yet, we believe that our study gives some general teachings on the mechanisms underlying spatial ordering at high pressures which would remain valid even in case some of the phases that we find stable are actually metastable.

As a preliminary test, we study the Lennard-Jones fluid at $T = 0$ and confirm that it can only exist in two forms, either as a hcp or as a fcc crystal, the former being stable at lower pressures [43]. The transition between the two occurs approximately at $P\sigma^3/\epsilon = 800$, though the chemical-potential difference is very small ($< 0.001\epsilon$) for all pressures up to 1000. Moreover, we find that apparently all Barlow packings are more stable than fcc for $P\sigma^3/\epsilon < 800$ while the metastable phase that is closest in stability to fcc is cI16 (with $x = 0.024$ at $P = 0$, slightly diminishing on increasing pressure), as suggested by the simulation [44]. We also verified that the only $T = 0$ phases of the GCM are fcc and bcc.

Table 2 collects the $T = 0$ phases of the exp-6 model with $\alpha = 11$. In Fig. 3, the chemical potential μ of the same phases is plotted as a function of pressure P , chosen fcc as reference (the units of length and energy are set to σ and ϵ , respectively). We do not show μ for all the scrutinized lattices since the difference in chemical potential between the stable and the

metastable phases is often very small on the scale of the picture, insomuch that it would have been difficult to keep track of all the curves. Examples of a strong competition between different phases are seen anyway in Fig. 3, near $P = 15000$ (hR1 vs. sh) and near $P = 35000$ (the challenge now being among oC8, hR1, sh, and wurtzite).

It transpires from Table 2 that the coordination number z has a regular trend with pressure. Starting from 12 (fcc-I) at low pressure, z reduces upon compression down to a minimum of 2 (hR1). Then, it increases progressively with pressure until becoming, eventually, 12 again (fcc-II). This behaviour can be rationalized as follows. We see from Table 2 that the nearest-neighbour distance is σ_M for all stable phases except for fcc-I and bcc-I. Whence the convenience, in order to minimize the energy at not too low pressure, that the number of first neighbours be as small as possible. Eventually, however, the PV term in the enthalpy takes over the energy and there will again be room for close-packed lattices. The reason why low-coordinated phases do not show up for systems with a Lennard-Jones-like potential is that, in these systems, the fcc and bcc crystals anyway manage to accomodate second and third neighbours at convenient distances. On the contrary, in systems interacting through soft-core potentials, fcc and bcc local orders are destabilized by the peculiar dependence of the interatomic force with distance, which, for high softness degrees, leads to the existence of two incommensurate length scales that heavily frustrate the too compact arrangements.

Looking at Fig. 3, a few other comments are in order: 1) the BC8 phase, which was previously [9] found to be stable for pressures between roughly 20000 and 30000, is actually less stable than βSn . 2) Interestingly, there are two distinct ranges of pressure where the exp-6 system exhibits oC8 order at $T = 0$. In fact, within one of these intervals there are phase transitions between different oC8 phases, as signalled by the jumps of parameters from one valley to another in parameter space. We tabulated up to four distinct oC8 phases for the exp-6 system though, actually, a careful examination of the data shows that the isostructural transitions, including the weaker ones, are many more. 3) In a wide pressure interval, the orthorhombic A20 lattice gives the most stable phase. There are actually five distinct A20 states at $T = 0$ with abrupt transitions between them at specific pressures. These transitions are in the form of unequal compressions along the b and c axes, also accompanied by an adjustment of the internal parameter y . 4) The change in slope which is manifest in all curves at $P \simeq 52000$ is due to a sudden change of the nearest-neighbour

distance of the optimal fcc crystal from roughly 0.406 down to $0.37381 = \sigma_M$ (a similar jump occurs for bcc at the same pressure). This effect is rather specific to the exp-6 system and ultimately related to the abrupt change of the potential profile at σ_M .

Table 3 reports the $T = 0$ phase diagram of the Yoshida-Kamakura potential. A comparison with the exp-6 case reveals a number of similarities as for the trend of coordination number with pressure and for the order of appearance of the phases. Hence, some of the considerations made for the exp-6 model also apply to this potential, in spite of the fact that the steepness of the Yoshida-Kamakura potential is a monotonous function of r (see Fig. 1). In Fig. 4, we show the discrete RDF of the $T = 0$ phases for u_{YK} . We see that, with the exception of the highest-pressure phases, the range of distances from a central particle that corresponds to the force “plateau” is void of neighbours, like as if particles tended to sit at the shortest distances available at same force strength. Something similar occurs for the exp-6 model, see Table 2, where no particles are found in the region of distances where the potential is concave.

We now try to obtain a rough phase diagram for the Yoshida-Kamakura model from just the knowledge of its $T = 0$ sector. The simplest way to do this is to lay down a (Lennard-Jones-Devonshire) cell theory [45] for the solid phases and to use the Lindemann criterion [46] for locating the melting transition. In the cell theory, a crystal partition function of effectively independent particles is written down where any given particle, which can be found anywhere in its own Wigner-Seitz cell (WSC), is acted upon by the force exerted by the other $N - 1$ particles, placed at their equilibrium lattice positions. In practice,

$$Z = \frac{1}{\Lambda^{3N}} \int_{\text{WSC}_1} d^3r_1 \cdots \int_{\text{WSC}_N} d^3r_N \exp \left\{ - \sum_i \phi(\mathbf{r}_i) / (k_B T) \right\}, \quad (4.11)$$

where

$$\phi(\mathbf{r}) = \frac{1}{2} \sum_{j \neq 1} u(|\mathbf{R}_1 - \mathbf{R}_j|) + \sum_{j \neq 1} [u(|\mathbf{R}_1 + \mathbf{r} - \mathbf{R}_j|) - u(|\mathbf{R}_1 - \mathbf{R}_j|)] \quad (4.12)$$

(we denote by capital letters the positions of lattice sites in the perfect crystal). Within this theory, the mean square displacement of a particle is given by

$$\langle \Delta r^2 \rangle = \frac{\int_{\text{WSC}} d^3r r^2 \exp\{-(\Phi(\mathbf{r}) - \Phi(0))/(k_B T)\}}{\int_{\text{WSC}} d^3r \exp\{-(\Phi(\mathbf{r}) - \Phi(0))/(k_B T)\}}, \quad (4.13)$$

for $\Phi(\mathbf{r}) = \sum_{j \neq 1} u(|\mathbf{R}_1 + \mathbf{r} - \mathbf{R}_j|)$. If we denote r_{NN} the nearest-neighbour distance, the Lindemann fraction is defined as

$$\mathcal{L} = \frac{\sqrt{\langle \Delta r^2 \rangle}}{r_{NN}}, \quad (4.14)$$

which is an increasing function of temperature. The Lindemann rule then states that melting occurs at the temperature T_m where \mathcal{L} reaches a critical value \mathcal{L}_c specific of the given lattice. Experience with other models shows that $\mathcal{L}_c = 0.15 \div 0.16$ for fcc and $0.18 \div 0.19$ for bcc [47] while, to our knowledge at least, there is no general consensus in the literature as to the value of \mathcal{L}_c for other lattices (we tentatively assume $\mathcal{L}_c = 0.19$).

Fig. 5 shows the phase diagram of the Yoshida-Kamakura potential as mapped out in the way just explained. Aside from the simplicity of the theory used, in plotting this figure we make two further assumptions: 1) We discard the possibility that some other phases, not stable at $T = 0$, might be promoted entropically for $T > 0$; 2) we exclude that a given phase might invade, for $T > 0$, the density intervals where the adjacent phases are stable for $T = 0$. Looking at Fig. 5, we see at least one region of reentrant melting between bcc-I and sh-I, but probably there are others. This is a curious finding in view of the absence of two clearly-defined repulsive length scales for this potential (by contrast, reentrant-fluid behaviour is well-documented for the exp-6 model [9] and the Fomin potential [24], both strongly-soft potentials). Since we do not calculate the phonon spectrum of the solids, we cannot exclude that some of them are actually mechanically unstable for $T > 0$. However, indirect clue to mechanical stability of a crystal phase can be the positive value of the elastic constant K associated with the one-particle potential $\Phi(\mathbf{r})$. This quantity can be extracted from the $\mathcal{O}(r^2)$ term in $\Phi(\mathbf{r})$, via a spherical average [23]. We have checked that, at least within the range of stability of each phase in Table 3, the value of K is always positive. Moreover, if we estimate the mean square displacement of a particle from the harmonic approximation for $\Phi(\mathbf{r})$, the resulting phase diagram comes out not too different from that of Fig. 5.

The $T = 0$ phase diagram of the Fomin potential is outlined in Table 4. We see the same trend of z with pressure as observed in the previous cases. However, we find only one non-Bravais phase in this case (βSn) which turns out to be almost degenerate with the bct phase throughout the whole pressure range from 3.5 to 5.5. All in all, the phase behaviour of unbounded soft-core potentials has some recurrent features (e.g. rich solid polymorphism, low-coordinated non-Bravais crystal phases, and reentrant melting) which are also found in the phase diagram of many simple elements under extreme conditions. This suggests that the effective two-body (adiabatic) potential of these substances is a soft-core potential.

Finally, we analyse the $T = 0$ phase diagram of the Hertz potential, Eq. (2.4), as sum-

marized in Table 5. A rather complex behaviour shows up for this bounded potential, much more complex than reported in [25], especially if compared with the simple phase portrait of the GCM. In fact, the phases listed in Table 5 are only those stable for $P < 400$ since apparently the sequence of $T = 0$ phase transitions never comes to an end (as observed in Ref. [25], there is no room for clustering in the Hertz model). This unique behaviour, never documented before, is the effect of a complex interplay between energy and volume considerations in the minimization of enthalpy as a function of pressure. Probably, this behaviour is related to the absence of a force plateau at $r = 0$ which obliges the system to continuously setting right the positions of the neighbouring particles.

V. CONCLUSIONS

In recent years, increasing attention has been devoted to soft-matter systems as examples of anomalous thermodynamic behaviour, both in and out of equilibrium. This field of research is very much alive, with many points of contact with high-pressure physics [9]. We have been focused here on the anomalously rich solid polymorphism of systems of softly-repulsive particles, by studying the zero-temperature phase diagram of a number of model pair potentials with various forms of core softening. We found elements of complexity that are simply unknown to “normal” fluids interacting through a Lennard-Jones type of potential, with many low-coordinated non-Bravais lattices providing the structure of stable phases at intermediate pressures. In a near future, with the advent of new techniques to functionalize the colloidal surface, one can expect to obtain colloidal systems whose soft-core potential yields spontaneous assembling into similar exotic lattices. The relation of solid polymorphism to other kinds of thermodynamic oddities, such as reentrant melting and water-like anomalies, is the subject of work in progress.

Acknowledgements

We acknowledge useful discussions with Ezio Bruno and Sandro Scandolo. We also thank an anonymous Referee of our previous paper [9] for driving our attention to the papers

[21, 22, 23].

[*] E-mail: Santi.Prestipino@unime.it

[†] E-mail: saija@me.cnr.it

[‡] E-mail: malescio@unime.it

- [1] C. N. Likos, *Phys. Rep.* **348**, 267 (2001).
- [2] G. Malescio, *J. Phys.: Condens. Matter* **19**, 073101 (2007).
- [3] M. Watzlawek, C. N. Likos, and H. Löwen, *Phys. Rev. Lett.* **82**, 5289 (1999).
- [4] C. N. Likos, N. Hoffmann, H. Löwen, and A. A. Louis, *J. Phys.: Condens. Matter* **14**, 7681 (2002).
- [5] A. A. Louis, P. G. Bolhuis, J. P. Hansen, and E. J. Meijer, *Phys. Rev. Lett.* **85**, 2522 (2000).
- [6] F. H. Stillinger, *J. Chem. Phys.* **65**, 3968 (1976).
- [7] A. Lang, C. N. Likos, M. Watzlawek, and H. Löwen, *J. Phys.: Condens. Matter* **12**, 5087 (2000).
- [8] S. Prestipino, F. Saija, and P. V. Giaquinta, *Phys. Rev. E* **71**, 050102(R) (2005).
- [9] G. Malescio, F. Saija, and S. Prestipino, *J. Chem. Phys.* **129**, 241101 (2008).
- [10] A. B. Migdal, *Sov. Phys. JETP* **7**, 996 (1958).
- [11] R. A. Buckingham, *Proc. R. Soc. London, Ser. A* **168**, 264 (1938).
- [12] M. Ross and A. K. McMahan, *Phys. Rev. B* **21**, 1658 (1980).
- [13] F. Saija and S. Prestipino, *Phys. Rev. B* **72**, 024113 (2005).
- [14] M. Ross, R. Boehler, and P. Söderlind, *Phys. Rev. Lett.* **95**, 257801 (2005).
- [15] See e.g. M. I. McMahon and R. J. Nelmes, *Chem. Soc. Rev.* **35**, 943 (2006).
- [16] D. Gottwald, C. N. Likos, G. Kahl, and H. Löwen, *Phys. Rev. Lett.* **92**, 068301 (2004).
- [17] D. Gottwald, G. Kahl, and C. N. Likos, *J. Chem. Phys.* **122**, 204503 (2005).
- [18] J. Fornleitner and G. Kahl, *Europhys. Lett.* **82**, 18001 (2008).
- [19] G. J. Pauschenwein and G. Kahl, *Soft Matter* **4**, 1396 (2008).
- [20] G. J. Pauschenwein and G. Kahl, *J. Chem. Phys.* **129**, 174107 (2008).
- [21] T. Yoshida and S. Kamakura, *Prog. Theor. Phys.* **47**, 1801 (1972).
- [22] S. Kamakura and T. Yoshida, *Prog. Theor. Phys.* **48**, 2110 (1972).
- [23] T. Yoshida and S. Kamakura, *Prog. Theor. Phys.* **56**, 330 (1976).

- [24] Yu. D. Fomin, N. V. Gribova, V. N. Ryzhov, S. M. Stishov, and D. Frenkel, *J. Chem. Phys.* **129**, 064512 (2008).
- [25] J. C. Pàmies, A. Cacciuto, and D. Frenkel, `cond-mat/0811.2227`
- [26] S. Prestipino, F. Saija, and P. V. Giaquinta, *J. Chem. Phys.* **123**, 144110 (2005).
- [27] See e.g. D. Frenkel and B. Smit, *Understanding molecular simulation* (Academic, New York, 2001).
- [28] J. Behler, R. Martoňák, D. Donadio, and M. Parrinello, *Phys. Rev. Lett.* **100**, 185501 (2008).
- [29] T. Ishikawa, A. Ichikawa, H. Nagara, M. Geshi, K. Kusakabe, and N. Suzuki, *Phys. Rev. B* **77**, 020101(R) (2008).
- [30] A. R. Oganov and C. W. Glass, *J. Chem. Phys.* **124**, 244704 (2006).
- [31] Y. Yao, J. S. Tse, Z. Song, D. D. Klug, J. Sun, and Y. Le Page, *Phys. Rev. B* **78**, 054506 (2008).
- [32] N. L. Abraham and M. I. J. Probert, *Phys. Rev. B* **77**, 134117 (2008).
- [33] Useful information about a wealth of crystal lattices can be found at <http://cst-www.nrl.navy.mil/lattice/index.html>
- [34] M. I. McMahon and R. J. Nelmes, *Phys. Rev. B* **47**, 8337 (1993).
- [35] U. Schwarz, K. Takemura, M. Hanfland, and K. Syassen, *Phys. Rev. Lett.* **81**, 2711 (1998).
- [36] A. W. Overhauser, *Phys. Rev. Lett.* **53**, 64 (1984).
- [37] M. Hanfland, K. Syassen, N. E. Christensen, and D. L. Novikov, *Nature* **408**, 174 (2000).
- [38] M. I. McMahon, E. Gregoryanz, L. F. Lundegaard, I. Loa, C. Guillaume, R. J. Nelmes, A. K. Kleppe, M. Amboage, H. Wilhelm, and A. P. Jephcoat, *Proc. Natl. Acad. Sci. U.S.A.* **104**, 17297 (2007).
- [39] E. Gregoryanz, L. F. Lundegaard, M. I. McMahon, C. Guillaume, R. J. Nelmes, and M. Mezouar, *Science* **320**, 1054 (2008).
- [40] J. B. Neaton and N. W. Ashcroft, *Nature* **400**, 117 (1999).
- [41] N. E. Christensen and D. L. Novikov, *J. Phys.: Condens. Matter* **14**, 10879 (2002).
- [42] H. Fujihisa, Y. Nakamoto, K. Shimizu, T. Yabuuchi, and Y. Gotoh, *Phys. Rev. Lett.* **101**, 095503 (2008).
- [43] A. N. Jackson, A. D. Bruce, and G. J. Ackland, *Phys. Rev. E* **65**, 036710 (2002).
- [44] H. Eshet, F. Bruneval, and M. Parrinello, *J. Chem. Phys.* **129**, 026101 (2008).
- [45] J. E. Lennard-Jones and A. F. Devonshire, *Proc. Roy. Soc. A* **163**, 53 (1937).

- [46] F. A. Lindemann, *Z. Phys.* **11**, 609 (1910).
- [47] F. Saija, S. Prestipino, and P. V. Giaquinta, *J. Chem. Phys.* **124**, 244504 (2006).

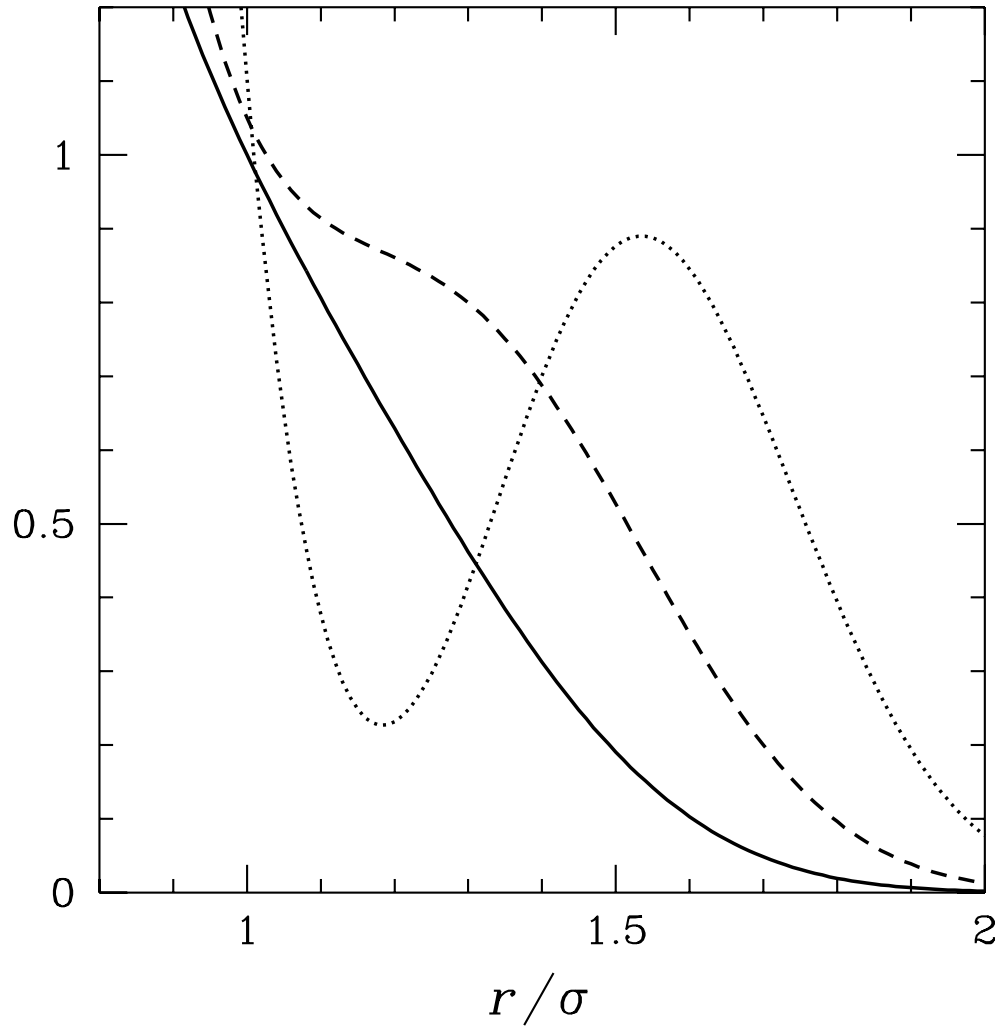


FIG. 1: Yoshida-Kamakura potential for $a = 2.1$ (solid line, in units of ϵ). The figure reports also the force (dashed line, in units of ϵ/σ) and the second derivative of the potential (dotted line, in units of ϵ/σ^2). Note that the force and its steepness have been divided by two and four, respectively, in order to fit into the picture.

TABLE I: The non-Bravais lattices that have been considered in our search for stable phases at zero temperature. For each structure (column 1), the parameter(s) which are needed for a complete specification of the lattice are reported in column 2. The symbols in this column have the same meaning as in the web site of Ref. [33], except for *Imma* [34] and oC16-Cs [35]. The number of inequivalent sites (NIS, see main text) of the given lattice is also indicated in column 3. For Bravais lattices, the parameters are axial ratios ($b/a, c/a$) and angles (α, β, γ), as usual.

lattice	parameters	NIS (with weights, if different)
hcp	—	1
dhcp	—	2
thcp	—	2 ($1 \times 1, 2 \times 2$)
9R	—	2 ($1 \times 1, 2 \times 2$)
diamond	—	1
fluorite	—	2 ($1 \times 1, 2 \times 2$)
A15	—	2 ($1 \times 1, 2 \times 3$)
bcc12	—	1
β Sn	c/a	1
cI16-Li	x	1
BC8	x	1
graphite	c/a	2
wurtzite	$(c/a)/\sqrt{8/3}, u/(3/8)$	1
<i>Imma</i>	$c/a, \Delta$	3 ($1 \times 1, 2 \times 1, 3 \times 2$)
B10	$c/a, z$	1
A7	$b/a, u$	1
A8	$c/a, x$	1
A13	x_1, x_2	2 ($1 \times 2, 2 \times 3$)
C6	$c/a, z$	2 ($1 \times 1, 2 \times 2$)
A20	$b/a, c/a, y$	1
oC8-Ga	$(b/a)/1.69479, c/a, u/0.1549, v/0.0810$	1
oC16-Cs	$(b/a)/0.594, (c/a)/0.590, x/0.2118, y/0.1781, z/0.328$	2
ST12	$c/a, x_1/0.0912, x_2/0.1730, y_2/0.3784, z_2/0.2486$	2 ($1 \times 1, 2 \times 2$)

TABLE II: Exp-6 potential for $\alpha = 11$: Zero-temperature phase diagram. For each phase (column 2), we show the pressure interval of stability (column 1), the related density interval (column 3), the first- and second-neighbour distances (column 4), the number of first- and second-neighbours (column 5), and the values of structure parameters (column 6).

P_1-P_2 ($10^3 \epsilon \sigma^{-3}$)	phase	$\rho_1-\rho_2$ (σ^{-3})	r_1 (σ) r_2 (σ)	z_1 z_2	parameters
0–5.5	fcc-I	1.627–6.943	0.58838–0.95435 0.83209–1.34966	12 6	—
5.6–11.8	bcc	6.999–9.267	0.51947–0.57042 0.59983–0.65867	8 6	—
11.9–17.1	hR1	10.123–11.500	0.37381 0.53305–0.56628	2 6	$-0.227 \div -0.220$
17.2–20.4	oC8-I	11.982–12.676	0.37381 0.52352–0.54667	$\simeq 3$ 2	$0.85 \div 0.91, 1.24 \div 1.38,$ $0.61 \div 0.63, 2.06 \div 2.24$
20.5–33.3	β Sn	13.455–15.445	0.37381 0.52989–0.57802	4 $4 \div 12$	$0.758 \div 0.986$
33.4–36.9	oC8-II	16.464–16.722	0.37381 0.50274–0.50809	$\simeq 5$ 2	$1.10 \div 1.15, 1.81 \div 1.85,$ $1.02 \div 1.04, 1.30 \div 1.34$
37.0–45.3	oC8-III	18.561–18.651	0.37381 0.54346–0.55677	$\simeq 7$ 2	$0.95 \div 0.98, 1.08 \div 1.09,$ $1.10 \div 1.12, 1.17 \div 1.23$
45.4–47.6	oC8-IV	19.097	0.37381, 0.51223	$\simeq 7, 2$	0.88, 1.11, 1.17, 1.33
47.7–48.2	A20-I	19.642	0.37381, 0.56016	$\simeq 8, 4$	1.726, 0.666, 0.167
48.3–52.1	A20-II	19.905	0.37381, 0.54115	$\simeq 8, 4$	1.522, 0.629, 0.179
52.2–52.8	A20-III	20.074	0.37381, 0.53498	$\simeq 8, 4$	1.468, 0.621, 0.183
52.9–57.3	A20-IV	20.383	0.37381, 0.52665	$\simeq 8, 4$	1.398, 0.610, 0.189
57.4–60.9	A20-V	20.813	0.37381, 0.51700	$\simeq 8, 4$	1.327, 0.601, 0.196
61.0–68.3	sh	22.107	0.37381, 0.52864	8, 12	1
68.4–76.9	wurtzite	24.337	0.37381, 0.52864	10, 9	2.225, 0.734
77.0–	fcc-II	27.075	0.37381, 0.52864	12, 6	—

TABLE III: Yoshida-Kamakura potential for $a = 2.1$: Zero-temperature phase diagram. Notations are the same as in Table 2.

P_1-P_2 ($\epsilon\sigma^{-3}$)	phase	$\rho_1-\rho_2$ (σ^{-3})	r_1 (σ)	z	parameters
0–0.63	fcc-I	0–0.325	1.63259–	12	—
0.64–1.26	bcc-I	0.331–0.415	1.46282–1.57736	8	—
1.27–2.29	sh-I	0.486–0.594	0.90256–0.99613	2	$0.615 \div 0.645$
2.30–2.55	A7	0.614–0.637	0.95415–0.96971	3	$3.962 \div 3.975$, $0.181 \div 0.184$
2.56–4.91	diamond	0.670–0.845	0.91603–0.98970	4	—
4.92–5.46	sh-II	0.908–0.944	0.95874–0.97289	6	$1.381 \div 1.388$
5.47–12.07	A20	0.985–1.322	0.90053–0.97273	$\simeq 8$	$1.728 \div 1.731$, $0.626 \div 0.646$, 0.167
12.08–15.68	hcp-I	1.424–1.583	0.96311–0.99770	12	—
15.69–52.75	bcc-II	1.593–2.618	0.79168–0.93426	8	—
52.76–138.28	fcc-II	2.629–4.024	0.70570–0.81328	12	—
138.29–365.65	hcp-II	4.026–6.075	0.61516–0.70558	12	—
365.66–	fcc-III	6.077–	–0.61509	12	—

TABLE IV: Fomin potential for $r_0 = 1.35\sigma$: Zero-temperature phase diagram. Phases with 5 parameters were not included in our scrutiny. Notations are the same as in Table 2.

P_1-P_2 ($\epsilon\sigma^{-3}$)	phase	$\rho_1-\rho_2$ (σ^{-3})	r_1 (σ)	z	parameters
0–3.12	fcc-I	0–0.468	1.44574–	12	—
3.13–3.55	bco	0.549–0.559	1.07840–1.08786	2	$1.326 \div 1.330$, $2.134 \div 2.145$
3.56–4.62	bct	0.655–0.680	1.08276–1.09938	4	$2.298 \div 2.317$
4.63–5.54	β Sn	0.690–0.708	1.05191–1.06223	4	$0.729 \div 0.733$
5.55–8.91	sc	0.801–0.859	1.05197–1.07677	6	—
8.92–14.88	sh	0.940–1.017	1.03906–1.06239	$\simeq 8$	$0.988 \div 0.994$
14.89–	fcc-II	1.166–	–1.06645	12	—

TABLE V: Hertz potential: Zero-temperature phases up to $P = 400$. For $P > 40$, only phases with 0 and 1 parameters were examined. Notations are the same as in Table 2.

P_1 – P_2 ($\epsilon\sigma^{-3}$)	phase	ρ_1 – ρ_2 (σ^{-3})	r_1 (σ)	z	parameters
0–0.49	fcc-I	0–2.211	0.86161–	12	—
0.50–1.70	bcc-I	2.287–3.447	0.72232–0.82817	8	—
1.71–2.45	sh-I	3.694–4.231	0.57655–0.60419	2	$0.838 \div 0.840$
2.46–3.96	cI16-I	4.353–5.249	0.51263–0.54563	3	0.125
3.97–5.73	β Sn-I	5.485–6.386	0.50503–0.52598	4	$2.416 \div 2.508$
5.74–7.20	bct-I	6.456–7.116	0.45974–0.46571	2	$0.571 \div 0.588$
7.21–10.61	A20-I	7.366–8.651	0.48857–0.51514	$\simeq 6$	$1.730 \div 1.731$, $0.719 \div 0.728$, 0.167
10.62–11.10	fluorite	8.745–8.910	0.47819–0.48118	8×1 , 4×2	—
11.11–11.57	fcc-II	9.050–9.214	0.53541–0.53863	12	—
11.58–14.63	A20-II	9.331–10.309	0.49960–0.51378	$\simeq 6$	1.731 , $1.448 \div 1.475$, 0.167
14.64–28.14	bcc-II	10.450–13.895	0.45386–0.49908	8	—
28.15–28.64	β Sn-II	14.093–14.202	0.40956–0.41061	4	0.578
28.65–38.10	sh-II	14.254–16.214	0.38467–0.40155	6	$0.894 \div 0.895$
38.11–54.07	sc	16.417–19.265	0.37303–0.39346	6	—
54.08–58.89	hR1-II	19.431–20.218	0.37193–0.37660	6	$-0.074 \div -0.072$
58.90–75.02	bct-II	20.312–22.789	0.32347–0.33647	2	$0.617 \div 0.622$
75.03–102.78	hR1-III	22.951–26.643	0.34178–0.36507	6	$0.543 \div 0.553$
102.79–141.62	hcp	26.905–31.323	0.35608–0.37459	12	—
141.63–148.08	bct-III	31.413–32.096	0.34382–0.34639	8	$0.916 \div 0.923$
148.09–169.07	bct-IV	32.121–34.248	0.33691–0.34488	8	$1.116 \div 1.155$
169.08–206.32	bct-V	34.328–37.754	0.31071–0.32268	4	$1.734 \div 1.766$
206.33–242.37	bcc12	37.822–40.873	0.31085–0.31900	8	—
242.38–307.75	hR1-IV	41.044–46.081	0.28614–0.30195	6	$0.130 \div 0.171$
307.76–345.22	hR1-V	46.113–48.746	0.27802–0.28422	6	$0.098 \div 0.110$
345.23–370.23	β Sn-III	48.859–50.541	0.27074–0.27429	4	$3.967 \div 3.988$
370.24–400	cI16-II	50.669–52.602	0.25402–0.25721	3	0.078

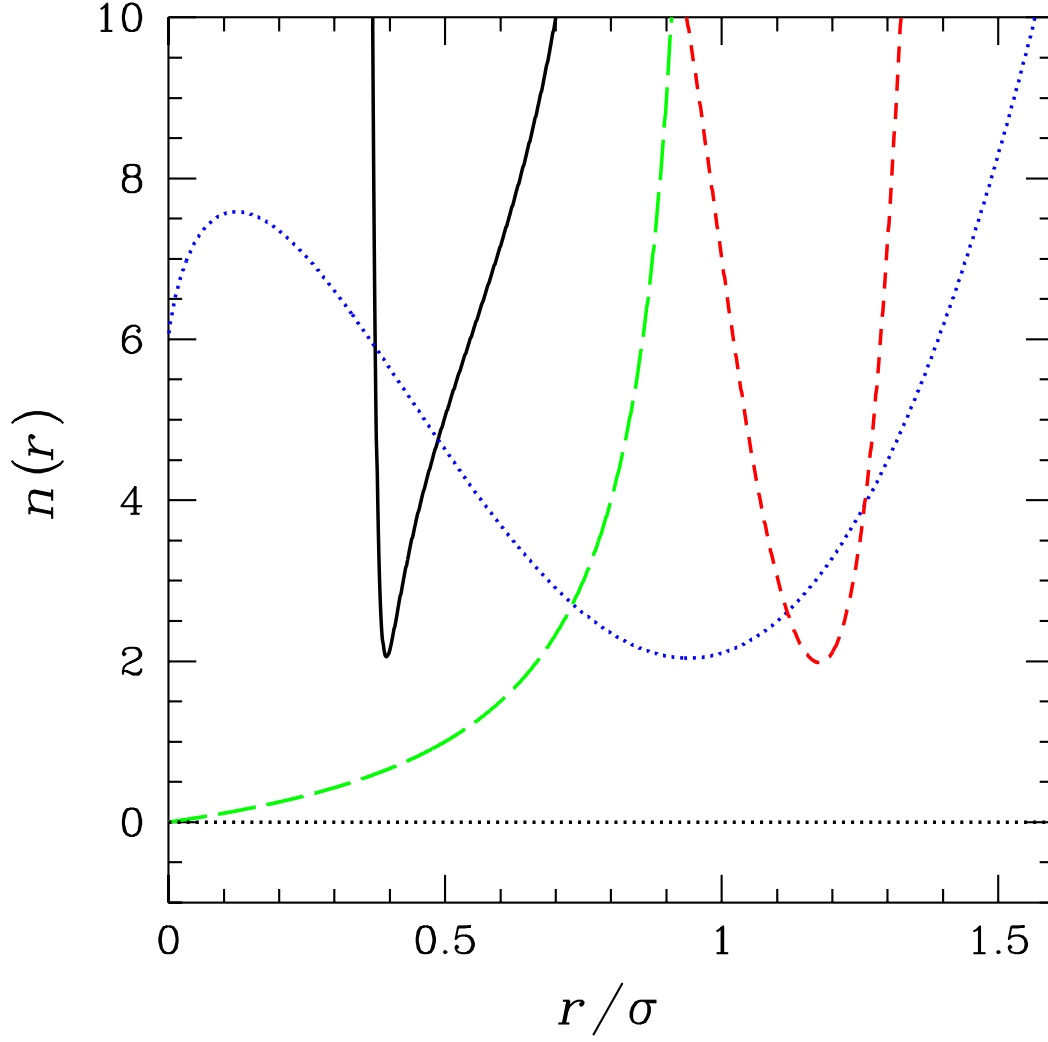


FIG. 2: (Color online) Effective inverse-power exponent $n(r)$ for the potentials (2.1)-(2.4), see Eq. (2.5): Exp-6 potential (solid line), Yoshida-Kamakura potential (dotted line), Fomin potential (dashed line), and Hertz potential (long-dashed line). For the exp-6 case, $n(r)$ was plotted only for those r where $u_E(r) > 0$.

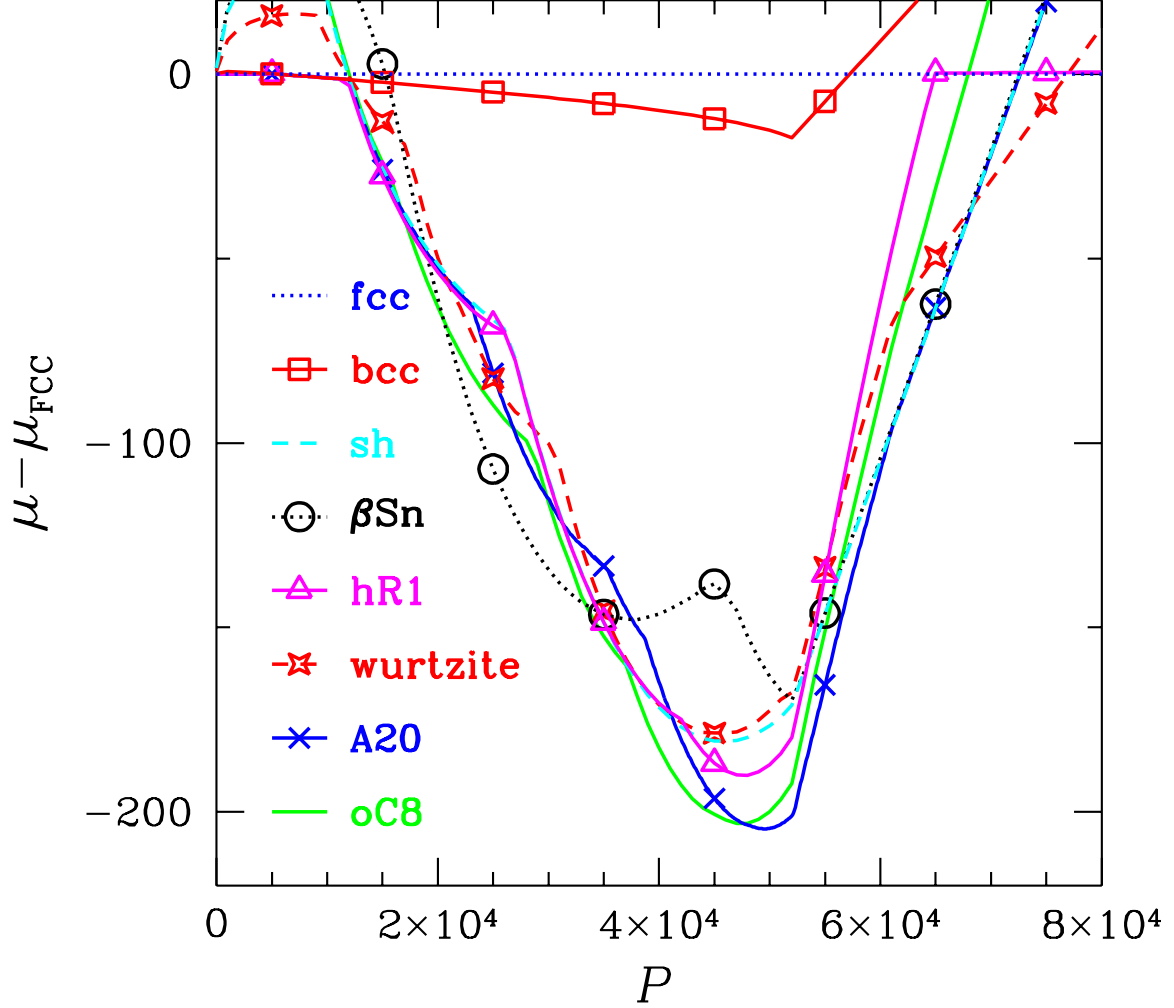


FIG. 3: (Color online) Exp-6 potential for $\alpha = 11$: $T = 0$ chemical potential μ , plotted as a function of pressure P , for a number of crystal structures, choosing the fcc lattice as reference (both μ and P are in reduced units; the chemical potentials of structures that are never stable are not shown). Besides fcc, the stable phases are bcc (squares and solid line), hR1 (triangles and solid line), β Sn (dots and dotted line), oC8 (solid line), A20 (crosses and solid line), sh (dashed line), and wurtzite (starred crosses and red dashed line).

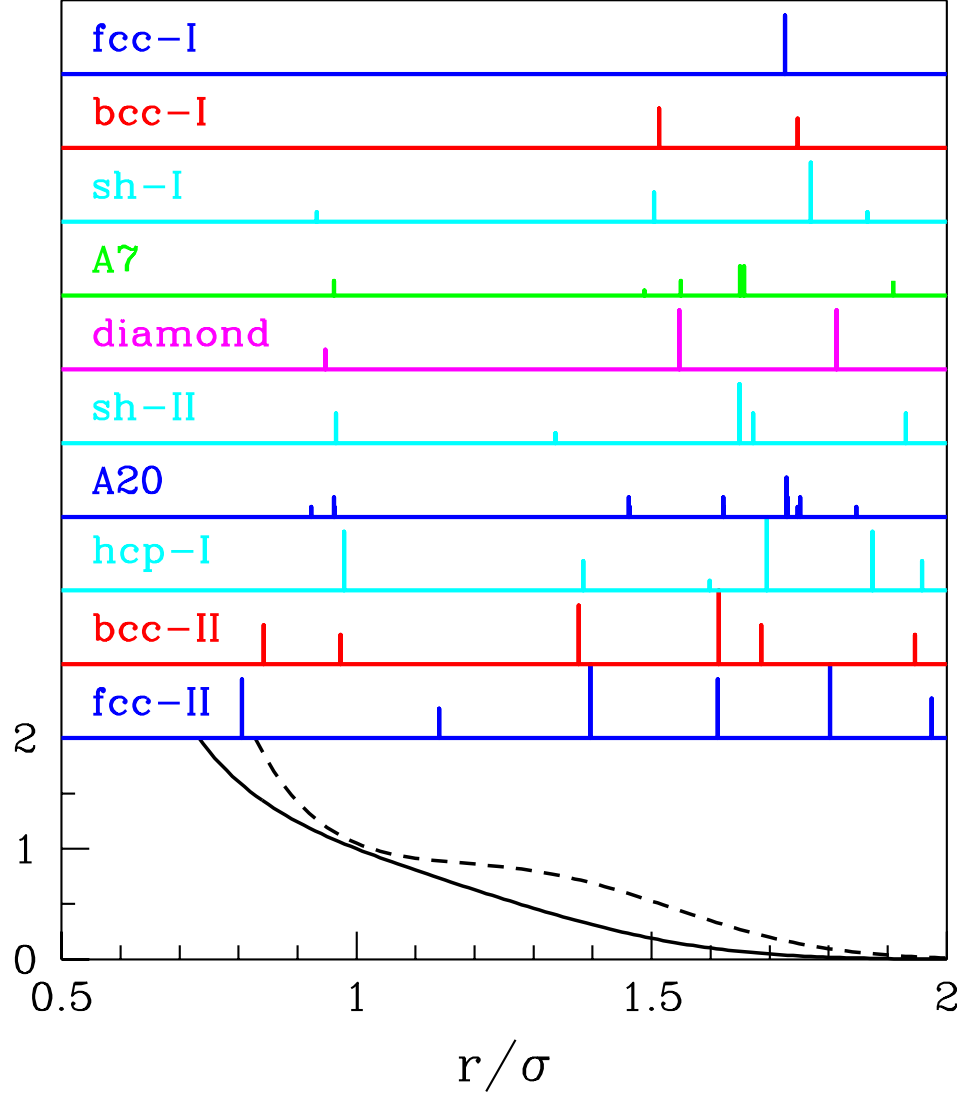


FIG. 4: (Color online) Yoshida-Kamakura potential: Comparison of the discrete radial distribution function for the various zero-temperature phases (the highest-pressure hcp-II and fcc-III phases are not shown). At every distance, this function simply counts the number of neighbours at that distance. The height of each panel is 15. Bottom panel: the potential (solid line) and the corresponding force divided by two (dashed line). From top to bottom: fcc-I ($P = 0.32$), bcc-I ($P = 0.95$), sh-I ($P = 1.79$), A7 ($P = 2.43$), diamond ($P = 3.73$), sh-II ($P = 5.19$), A20 ($P = 8.77$), hcp-I ($P = 13.88$), bcc-II ($P = 34$), and fcc-II ($P = 56$).

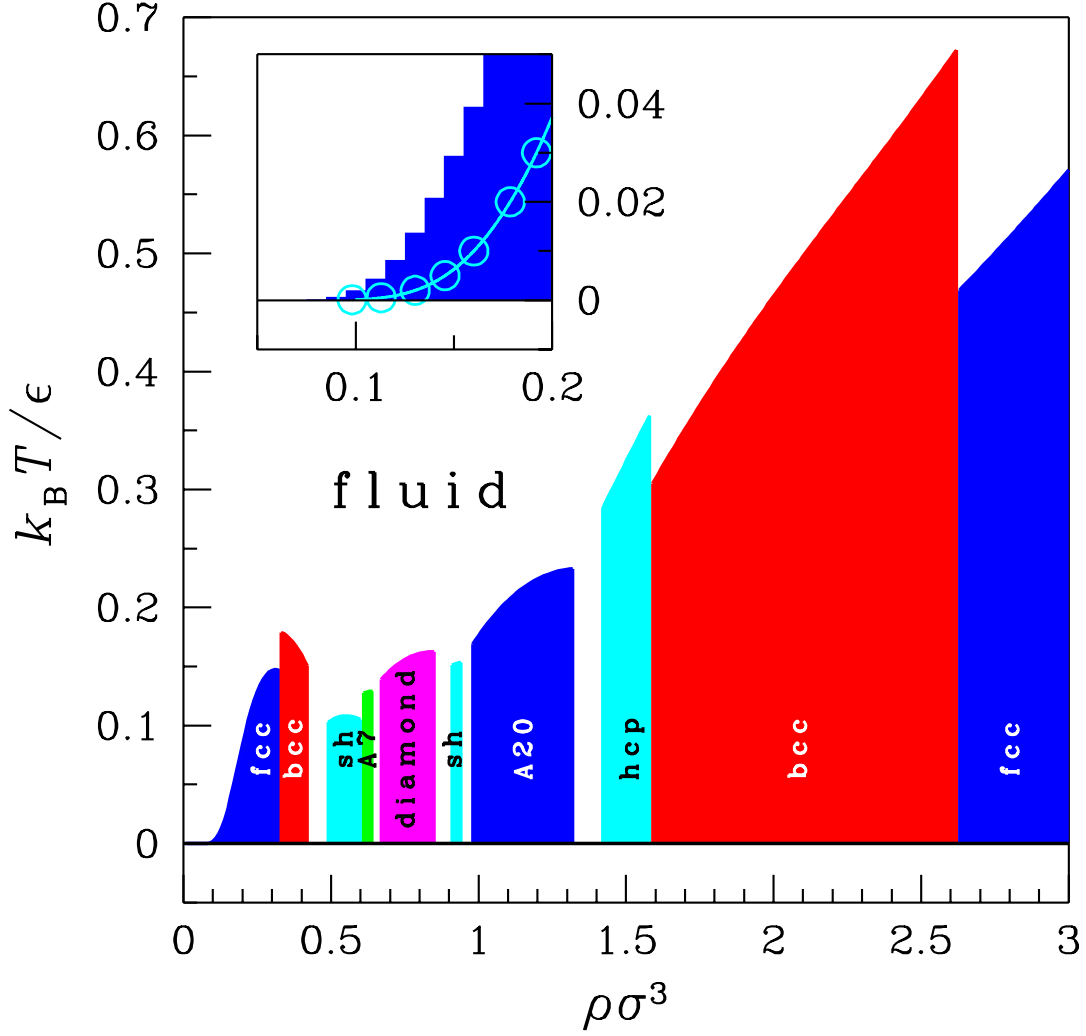


FIG. 5: (Color online) Yoshida-Kamakura potential: Schematic phase diagram in the ρ - T plane up to $\rho\sigma^3 = 3$, as obtained by combining the cell theory for the $T = 0$ solids with the Lindemann rule. Density gaps between the phases are two-phase coexistence regions. In the low-density region, the prediction of Eq. (2.10) for the fcc melting line (open dots) is compared with that based on the Lindemann criterion.